Mon. Not. R. Astron. Soc. **387,** 1080–1092 (2008) doi:10.1111/j.1365-2966.2008.13117.x

Sh2-205 – I. The surrounding interstellar medium

G. A. Romero[1,2]★ and C. E. Cappa[1,2]

[1]*Instituto Argentino de Radioastronomía, CC 5, 1894 Villa Elisa, Argentina*
[2]*Facultad de Ciencias Astronómicas y Geofísicas, Universidad Nacional de La Plata, Paseo del Bosque s/n, 1900 La Plata, Argentina*

Accepted 2008 February 15. Received 2008 February 14; in original form 2007 December 18

ABSTRACT

We investigate the distribution of the interstellar matter in the environs of the H II region Sh2-205, based on neutral hydrogen 21-cm-line data and radio continuum images at 408 and 1420 MHz obtained from the CGPS, ^{12}CO (J=1 →0) observations, high-resolution *IRAS* data (*HIRES*), and *MSX* data.

Sh2-205 can be separated into three distinct optical structures: SH 149.25–0.0, SH 148.83–0.67, and LBN 148.11–0.45. The three regions are detected at both 408 and 1420 MHz. The derived spectral indices show the thermal nature of SH 148.83–0.67 and LBN 148.11–0.45.

LBN 148.11–0.45 is a classical H II region surrounded by an H I shell. The associated neutral atomic and ionized masses are 65 $M_\odot$ and 70 $M_\odot$, respectively. Dust and molecular gas ($\sim 6 \times 10^4$ $M_\odot$) related to this ionized region have been found. In particular, a photodissociation region is detected at the interface between the ionized and molecular regions. If the proposed exciting star HD 24094 were an O8–O9 type star, as suggested by its near-infrared colours, its UV photon flux would be strong enough to explain the ionization of the nebula.

The optical, radio continuum, and 21-cm-line data allow us to conclude that SH 148.83–0.67 is an interstellar bubble powered by the energetic action of HD 24431. The associated neutral atomic and ionized masses are 180 $M_\odot$ and 300 $M_\odot$, respectively. The emission of SH 149.25–0.0 is too faint to derive the dust and gas parameters.

An H I shell centred at $(l, b) = (149^\circ 0', -1^\circ 30')$ was also identified. It correlates morphologically with the molecular gas emission. The neutral atomic and molecular masses of the shell are 1600 $M_\odot$ and 2.6×10^4 $M_\odot$, respectively. The open cluster NGC 1444 is probably responsible for shaping this H I structure.

Key words: stars: individual: HD 24431 – stars: individual: ALS 7793 – stars: individual: HD 24094 – ISM: bubbles - ISM: structure.

1 INTRODUCTION

O-type stars emit large numbers of UV photons capable of ionizing the neutral atomic gas and photodissociating molecular material, leading to the creation of H II regions (Osterbrock 1989) and of photodissociation regions at the interface between the ionized and the molecular gas (Hollenbach & Tielens 1997). H II regions evolve from ultracompact to classical regions, modifying the characteristics of their natal environment. They appear surrounded by neutral atomic and molecular gas, generally made up of the remains of their natal clouds. Subsequent dynamical expansion favours the formation of dense slowly expanding neutral envelopes behind front shocks (Spitzer 1978), where conditions for stellar formation may be fulfilled.

Massive stars also lose mass at rates of 10^{-6}–10^{-7} $M_\odot$ yr^{-1} with terminal velocities of 1000–2000 km s^{-1} (Prinja, Barlow & Howarth 1990; Chlebowski & Garmany 1991; Lamers & Leitherer 1993). Although clumpy stellar winds result in lower mass-loss rates (Moffat & Puls 2003), the huge amount of mechanical energy released into the interstellar medium (ISM) through the stellar wind mechanism during the lifetime of a massive star is capable of creating stellar wind bubbles. An outer dense neutral shell will appear between the outer shock front and the ionization front if this last front is trapped within the expanding bubble (Weaver et al. 1977; Lamers & Cassinelli 1999).

The action of massive stars on the surrounding ISM can be analysed using radio continuum data, which allow us to determine the characteristics of the ionized gas. Neutral hydrogen 21-cm-line emission and molecular data allow us to investigate the distribution of the neutral atomic and molecular gas in the environs of the stars, and interstellar dust characteristics can be studied through its infrared emission.

Massive stars are the main source of energy injection into the ISM in the Galaxy. This injection causes the redistribution of interstellar material by photodynamical and photochemical processes. In order

★E-mail: gisela@iar-conicet.gov.ar

to improve theoretical scenarios, it is necessary to carry out comprehensive observational studies. This is possible by undertaking complete multiwavelength studies of H II regions and interstellar bubbles.

In order to gain a better understanding of the ISM and the processes that modify it, we are carrying out a systematic study of the kinematics and energetics of the ionized and neutral gas in the environs of massive stars. In this paper we analyse the H II region Sh2-205 in the region of Camelopardalis, based on the radio continuum, the H I 21-cm line, the ^{12}CO line, and infrared data at several wavelengths.

2 THE H II REGIONS AND THEIR EXCITING STARS

Fig. 1 displays the Virginia Tech Spectral-Line Survey (VTSS) and Digitized Sky Survey-Red (DSS-R) images of a region of $\sim 2 \times 2\,\mathrm{deg}^2$ centred at $(l, b) = (148^\circ40', -0^\circ20')$, showing the H II region Sh2-205 (Sharpless 1959) of about 120 arcmin in size. The images reveal the presence of diffuse extended emission with two bright areas. One of them consists of an arc-like structure located at $(l, b) = (148^\circ45', -0^\circ50')$. The VTSS image shows that the edges

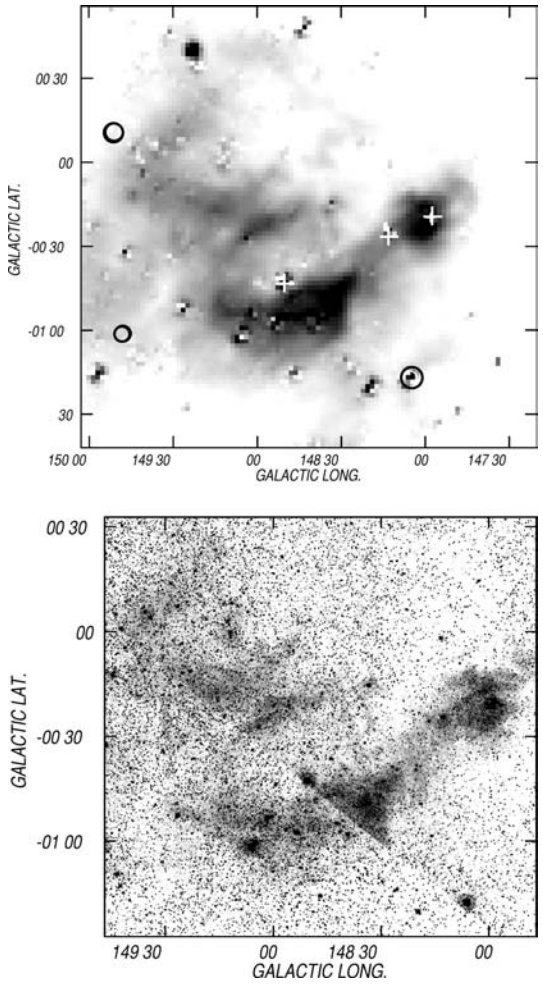

Figure 1. Optical images of the Sh2-205 H II region. (a) VTSS continuum-corrected Hα image. The positions of the stars HD 24431, ALS 7793, and HD 24094 are indicated by crosses. The locations of the open clusters NGC 1496, King 7 and NGC 1444 are marked by open circles. (b) DSS-R image of the region.

Table 1. Photometric and astrometric results for HD 24431, ALS 7793, and HD 24094.

HD 24431					
l (°)	b (°)	Spectral type	V_r(LSR) (km s^{-1})	Distance (pc)	Ref.
148°50′	−0°43′	O9 IV-V[1]	-9.9 ± 2[3]	957	4
		O9 III[2]		1000	3,5
				2280	6
ALS 7793					
l (°])	b (°)	Spectral type	m_v (mag)		
148°17′	−0°26′	B1 V[1]	11.1[1]		
HD 24094[7]					
l (°)	b (°)	Spectral type	P (days)	B-V (mag)	
147°58′	−0°20′	B8 V	1.052	0.4	

Notes: 1: Hiltner & Johnson (1956); 2: Walborn (1973); 3: Humphreys (1978); 4: Zdanavičius et al. (2001); 5: Gies (1987); Garmany et al. (1982); 6: Cruz-González et al. (1974); 7: Duerbeck (1997).

of this arc are brighter than the inner region. Along with the fainter optical emission region detected at $(l, b) \approx (149^\circ0', -0^\circ20')$, the arc-like feature delineates an almost complete shell centred at approximately $(l, b) = (148^\circ50', -0^\circ40')$, of ~ 60 arcmin in diameter. From here on, this structure will be referred to as SH 148.83–0.67.

The exciting star of this H II region is the O-type star HD 24431 (Sharpless 1959), located at $(l, b) = (148^\circ50', -0^\circ43')$, projected close to the centre of this structure. This star was classified as O9 IV-V by Hiltner & Johnson (1956) and as O9 III by Walborn (1973). Fabricius et al. (2002), based on Tycho2 data, identified this star as a double system.

Distance determinations for HD 24431 span the range from 710 to 1000 pc (Zdanavičius et al. 2001; Gies 1987; Garmany, Conti & Chiosi 1982; Humphreys 1978). Cruz-González et al. (1974) adopted a distance of 2.28 kpc, considering this star to be a member of χ Persei. However, this open cluster is located at $(l, b) = (135^\circ,-3^\circ36')$, 14° from HD 24431, making its association with the star doubtful.

Table 1 lists the main photometric and astrometric parameters of HD 24431 in the literature. Humphreys (1978) and Garmany et al. (1982) believed this star was related to Cam OB1 ($[l, b] = [142^\circ, +2^\circ]$ of $\sim 1.7 \times 10\,\mathrm{deg}^2$ in size). Lyder (2001) carried out an extensive analysis of the optically identified Population I objects in the Cam OB1 region, deriving a distance of 975 ± 90 pc for the OB association, and does not consider HD 24431 to be a member of Cam OB1. In what follows, we adopt a distance of $d = 1.0 \pm 0.2$ kpc for HD 24431, in agreement with previous determinations.

The other bright extended area shown in Fig. 1 is the conspicuous H II region centred at $(l, b) = (148^\circ5', -0^\circ28')$. This region was catalogued as LBN 148.11–0.45 ($43 \times 25\,\mathrm{arcmin}^2$ in size) by Lynds (1965), although it had originally been included in Sh2–205 by Sharpless (1959). Two B-type stars appear projected onto this region. One of them is ALS 7793 [$(l, b) = (148^\circ17', -0^\circ26')$], whose spectral type is B1 (Hiltner & Johnson 1956). This star is situated

on the border of the H II region. The other star, HD 24094 [CY Cam, $(l, b) = (147^\circ58', -0^\circ20')$], is seen projected near the centre of LBN 148.11–0.45. Based on the *Hipparcos* catalogue, HD 24094 was identified as a slowly pulsating contact binary by Duerbeck (1997), its primary component being classified as a B8 star. The main parameters of these stars are listed in Table 1. No information about the distances to HD 24094 and ALS 7793 is available. As a working hypothesis, we adopt $d = 1.0 \pm 0.2$ kpc.

Radio studies of the Sh2-205 H II region have been performed by several authors. Blitz, Fich & Stark (1982) detected a molecular component at -25 ± 1 km s^{-1} in their CO study of H II regions, pointing the telescope towards the position $(l, b) = (148^\circ50'.4, -1^\circ14'.4)$. Based on radio continuum data at 1400 MHz with an angular resolution of 10 arcmin, Felli & Churchwell (1972) found two radio sources. One of them, centred at $(l, b) = (147^\circ54', -0^\circ24')$, has a flux density of 7.4 Jy and is 30.7×22.7 arcmin^2 in size. This source coincides spatially with LBN 148.11–0.45. The other radio source was detected at $(l, b) = (148^\circ42', -0^\circ7')$, has a flux density of 0.2 Jy, and is 14×10.8 arcmin^2 in size. It appears projected onto a region almost free of optical emission.

No radial velocity information corresponding to the ionized gas in the bright regions is available. The only measurement comes from Fabry–Perot Hα observations obtained by Fich, Dahl & Treffers (1990), who found a radial velocity of -16.8 ± 0.3 km s^{-1} observing towards the position $(l, b) = (147^\circ55'.8, -0^\circ3'.46)$.

In addition to the above-mentioned optical features, a shell-like structure of faint diffuse optical emission has been detected centred at $(l, b) = (149^\circ15', 0^\circ)$ (hereafter SH 149.25–0.00), spread over a circle of $\sim1^\circ$ in size. No stellar object seems to be related to this feature. This structure, together with the one probably related to HD 24431, was catalogued as LBN 149.02–00.13 by Lynds (1965).

The positions of the open clusters NGC 1496 at $(l, b) = (149^\circ51', +0^\circ11')$, NGC 1444 at $(l, b) = (148^\circ6', -1^\circ18')$, and King 7 at $(l, b) = (149^\circ46', -1^\circ1')$ are indicated in the VTSS image. Their distances are 1.2 kpc (del Rio & Huestamendia 1988), 1.19 kpc (Lindoff 1968), and 2.2 kpc (Durgapal, Pandey & Mohan 1997), respectively. Although they are seen projected close to the regions under study, their physical relation to the optical nebulae is doubtful.

3 DATA SETS

Radio continuum images at 408 and 1420 MHz, and 21-cm H I line emission data were taken from the Canadian Galactic Plane Survey (CGPS) observed with the DRAO Synthesis Telescope, in Penticton, Canada. The CGPS is a high-resolution survey of atomic hydrogen and radio continuum emission from the Galaxy. The spectral line observations are presented as data-cubes with 272 spectral channels having a velocity resolution of 1.3 km s^{-1}. Table 2 presents the most important observational parameters of the DRAO data base (Taylor et al. 2003). The radio continuum images at 408 and 1420 MHz, and the H I line data-cube were spatially smoothed to an angular resolution of $\sim$2 arcmin.

The radio continuum image at 2695 MHz, obtained using the Effelsberg 100-m telescope with an angular resolution of about 4.3 arcmin and an rms noise of 0.05 K (Fürst et al. 1990), was also analysed.

Images in the mid- and far-infrared obtained with the *MSX* and *IRAS* satellites were used to investigate the dust emission distribution. The *MSX* data consist of images at 8.3 μm (band A), 12.1 μm (band C), 14.7 μm (band D), and 21.3 μm (band E), obtained with an angular resolution of 18.3 arcsec. The *IRAS* (*HIRES*)[1] data include images at 12, 25, 60, and 100 μm with angular resolutions in the range 0.5 to 2.0 arcmin. The *IRAS* images are included in the DRAO data set.

Table 2. DRAO data: observational parameters.

Parameter	Value
H I	
Synthesized beam	$1'.22 \times 0'.97$
rms noise (single channel) (K)	1.0
Bandwith [MHz]	1.0
Channel separation (km s^{-1})	0.82
Velocity resolution (km s^{-1})	1.3
Velocity range (km s^{-1})	$-165, +45$
1420 MHz	
Synthesized beam	$1'.03 \times 0'.96$
rms noise (K)	0.06
Bandwith (MHz)	30.0
408 MHz	
Synthesized beam	$3'.5 \times 2'.8$
rms noise (K)	0.4
Bandwith (MHz)	4.0

^{12}CO (J = 1 → 0) data from Dame, Hartmann & Thaddeus (2001) were used to analyse the molecular gas distribution in the region. These data have an angular resolution of 7.5 arcmin, a velocity resolution of 1.3 km s^{-1}, and an rms noise of 0.05 K.

4 THE GAS AND DUST DISTRIBUTIONS

4.1 The ionized gas

Fig. 2 shows the radio continuum emission distributions at 408 and 1420 MHz (upper panels), and overlays of the radio continuum emissions and the VTSS image (lower panels). The images at both frequencies show emission from LBN 148.11–0.45, and from the shell-like features at $(l, b) \approx (148^\circ50', -0^\circ40')$ and $(l, b) \approx (149^\circ15', -0^\circ)$.

The 1420-MHz radio continuum emission associated with LBN 148.11–0.45 is strong. It consists of an almost circular, centrally peaked region, of $\sim30 \times 24$ arcmin^2 in size. The radio peak at $(l, b) \approx (147^\circ59'.4, -0^\circ25')$ does not coincide with the maximum in optical emission at $(l, b) \approx (147^\circ58', -0^\circ19')$.

As regards SH 148.83–0.67 (related to HD 24431), the radio emission at 1420 MHz is smooth and very well defined, with the brighter optical region coincident with the highest radio continuum emission at $(l, b) \approx (148^\circ30', -0^\circ46')$. The borders of the optical arc are brighter than the inner region, with the radio image displaying a fairly uniform region instead. This radio emission extends towards the galactic plane, appearing as a diffuse and faint almost complete ring of 13 arcmin in width and 60 arcmin in diameter, which correlates with the diffuse optical emission in the shell. Owing to the lower angular resolution of the image at 408 MHz, the ring is not as well defined as it is at 1420 MHz. HD 24431 is seen projected onto the inner border of this ring, near to one of the bright optical emission regions.

[1] IPAC is funded by NASA as part of the *IRAS* extended mission under contract to the Jet Propulsion Laboratory (JPL) and California Institute of Technology (Caltech).

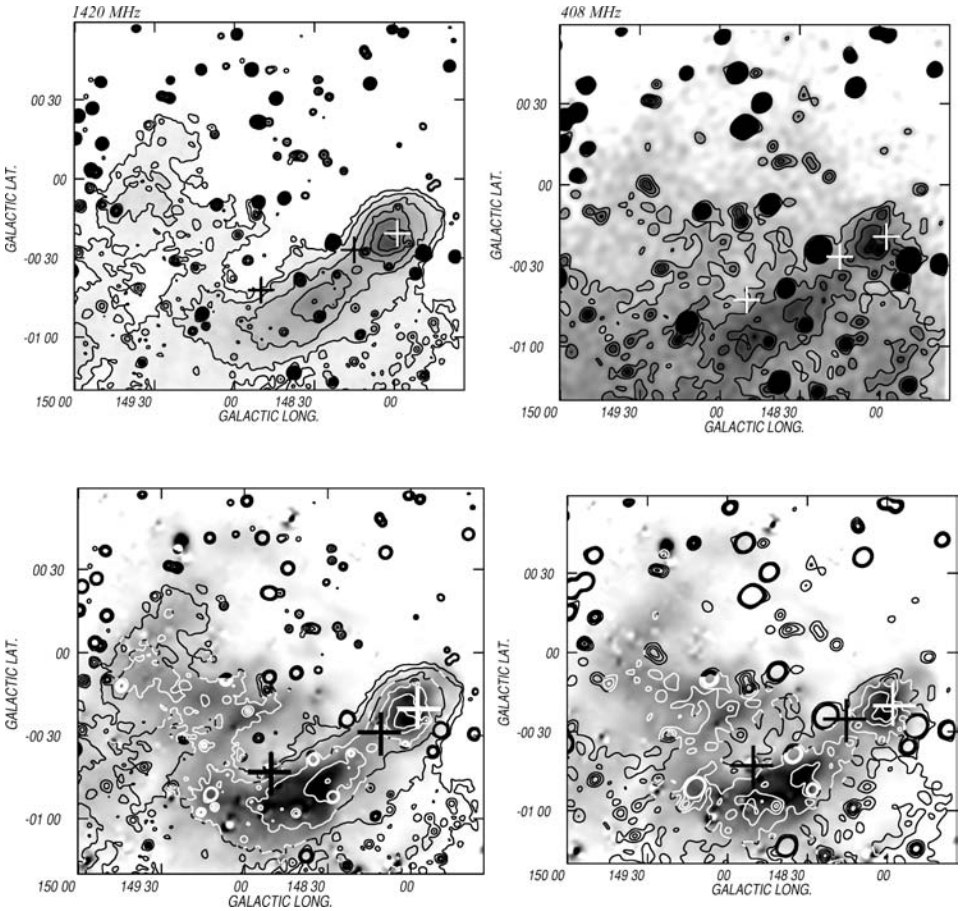

Figure 2. Radio continuum images at 1420 and 408 MHz. (a) Image at 1420 MHz. Contour levels are from 5.2 to 6.1 K in steps of 0.2 K. (b) Image at 408 MHz. Contour levels are from 53 to 61 K in steps of 2 K. (c) Overlay of the 1420-MHz image (contours) and the VTSS image. (d) Overlay of the 408-MHz image (contours) and the VTSS image.

The diffuse radio continuum emission also correlates with SH 149.25–0.00. It is not clear if the two shell-like features, namely SH 149.25–0.0 and SH 148.83–0.67, are linked.

As a first step in deriving the physical parameters of the extended radio structures, we have analysed the small-diameter sources projected onto and near the optical emission regions. Their galactic coordinates and derived flux densities measured at 1420 and 408 MHz are listed in Table 3. Their spectral indices α ($S_\nu \propto \nu^\alpha$) derived using fluxes at these frequencies are shown in the fifth column. The sixth column indicates previous references to the sources. The derived spectral indices indicate that all but two sources are non-thermal in nature. These results are reinforced by the fact that all sources are identified as extragalactic sources in the NASA Extragalactic Data base (NED). Two sources are particularly interesting. One of them, NRRF J035430.6+530759, is a galaxy. The other one, NVSS J035347+523208, has a steep spectral index (-2.27), and could correspond to a pulsar. However, this source is not listed in pulsar catalogues (see, for example, Taylor et al. 1993).

Flux densities at 2700, 1420 and 408 MHz for LBN 148.11–0.45 and SH 148.83–0.67, along with angular and linear sizes, are listed in Table 4. Flux densities corresponding to the small-diameter non-thermal sources were subtracted from the measured fluxes at 1420, 408 and 2700 MHz for the two nebulae. The expected flux density of the non-thermal sources at 2700 MHz was estimated from the spectral index. The spectral indices derived using the resulting flux densities at 408, 1420 and 2700 MHz are listed in Table 4, indicating that the emission originates in thermal bremsstrahlung. We note that the emission at 2700 MHz is very low and may lead to a large uncertainty in the estimate of the spectral index. By including the flux densities at 408 and 1420 MHz only, the spectral index results $\alpha = +0.14 \pm 0.02$ for SH 148.83–0.67 and $+0.4 \pm 0.04$ for LBN 148.11–0.45, also compatible with a thermal nature. Thus, the derived spectral indices show that the sources are thermal in nature.

The physical parameters of the H II regions, namely emission measure *EM*, electron density n_e, and ionized mass M_i, were obtained using the expressions given by Mezger & Henderson (1967) and correspond to a filling factor $f = 1$. For the case of SH 148.83–0.67, a more realistic volume filling factor was estimated considering a shell structure with inner radius R_{in} and outer radius R_{ou}. Both radii were measured using the radio continuum map at 1420 MHz, taking into account the contour level of 5.15 K ($\equiv 85\sigma$) (see Fig. 2). The values 28 and 13 arcmin were obtained for R_{ou} and R_{in}, respectively. For the adopted distance, $d = 1$ kpc, $R_{ou} = 8.2$ pc and $R_{in} = 3.8$ pc. Assuming that 10–30 per cent of the shell surface is occupied by plasma, the derived volume filling factor is in the range 0.1–0.3.

The assumed electron temperature is 10^4 K for the case of LBN 148.11–0.45, and values in the range $(0.6–1.0) \times 10^4$ K were used for SH 148.83–0.67. The derived ionized masses were multiplied by 1.27 to take into account singly ionized helium (Goss &

Table 3. Small-diameter sources projected onto the region.

Position l (°)	Position b (°)	S_{1420} (mJy)	S_{408} (mJy)	α	Source designation
		Sources seen on LBN 148.11–0.45			
147°49′	−0°28′	503 ± 0.93	1038 ± 18	−0.58 ± 0.03	NVSS J035125+532828
147°52′	−0°35′	80 ± 0.92	167 ± 17	−0.59 ± 0.17	NVSS J035107+532041
147°54′	−0°25′	13.3 ± 0.91	14 ± 10	−0.03 ± 1.25	NVSS J035205+532753
148°02′	−0°33′	19.9 ± 0.89	39 ± 21	−0.54 ± 0.92	NVSS J035210+531621
148°11′	−0°28′	21.2 ± 0.84	60 ± 32	−0.8 ± 0.2	NVSS J035320+531453
147°59′	−0°11′	13 ± 0.9	45 ± 27	−1.0 ± 0.2	NVSS J035327+533601
		Sources seen on SH 148.83–0.67			
148°23′	−0°24′	405.4 ± 1.5	1288 ± 19	−0.92 ± 0.02	NRRF J035430.6+530759
148°35′	−0°39′	59.2 ± 1.6	177 ± 20	−0.88 ± 0.16	6C B035049.0+524145
148°37′	−0°37′	17.8 ± 1.5	149 ± 62	−1.7 ± 0.6	NVSS J035337+530130
148°28′	−0°52′	70.9 ± 1.6	81 ± 19	−0.12 ± 0.38	87GB 034917.6+523604
148°22′	−0°47′	9.2 ± 1.8	17 ± 8	−0.48 ± 0.57	NVSS J035256+525159
148°16′	−0°58′	24.9 ± 1.6	14 ± 5	+0.47 ± 0.51	NVSS J035651+521521
149°12′	−0°51′	20.4 ± 1.5	419 ± 19	−0.57 ± 0.074	87GB 035303.4+520859
148°51′	−0°09′	123.4 ± 1.5	not resolved		87GB 035414.7+525443
148°52′	−0°14′	5.06 ± 0.32	18 ± 5	−1.01 ± 0.34	NVSS J035748+525933
148°59′	−0°21′	15.7 ± 1.5	35 ± 18	−0.64 ± 0.2	NVSS J035751+524924
148°41′	−0°58′	1.94 ± 0.25	33 ± 16	−2.27 ± 0.68	NVSS J035347+523208
148°13′	−0°59′	30.3 ± 1.9	30 ± 7	+0.01 ± 0.36	NVSS J035115+525046

Notes: Col. 6: References found in the NED catalogue: 6C, Hales, Baldwin & Warner (1988); NVSS, Condon et al. (1998); 87GB, Gregory & Condon (1991); NRRF, Newberg et al. (1999).

Lozinskaya 1995). The results are listed in Table 4. Uncertainties in masses and electron densities come mainly from the distance uncertainty. For the case of LBN 148.11–00.45, the central radio peak suggests $f = 1$.

4.2 Dust emission distribution

Fig. 3 illustrates the infrared emission distribution in the area under study. Part (a) displays the emission at 60 μm in contours and grey-scale, and part (b) shows an overlay of the infrared emission at 60 μm (grey-scale) and of the radio continuum emission at 1420 MHz (contours).

The emission distribution in the far-infrared differs from the radio continuum emission. Strong infrared emission comes from LBN 148.11–0.45. Arc-shaped extended emission at 60 μm strikingly surrounds the border of the H II region towards higher galactic longitudes, and separates this region from SH 148.83–0.67.

Two small emission regions are easily distinguished in LBN 148.11–0.45. One of them is a relatively extended feature coincident with the stellar position. This 60-μm maximum is shifted 5 arcmin from the maximum at 1420 MHz. The other infrared region is detected towards $(l, b) = (148°0′, -0°10′)$. Its position is coincident with the small-diameter source NVSS J035327+533601, detected in the radio continuum and suspected to be an extragalactic source.

Faint diffuse infrared emission also overlaps part of SH 148.83–0.67. This weak feature coincides with the arc-like structure seen at 1420 MHz and at optical wavelengths (see Fig. 2). No far-infrared emission is identified near $(l, b) = (149°00′, -0°20′)$, where faint optical emission belonging to SH 148.83–0.67 was detected.

The image at 100 μm is not shown here as the emission distribution is similar to that at 60 μm.

Fig. 3(c) shows an overlay of the infrared emission at 8.3 μm (band A of the *MSX* satellite) (grey-scale) and the infrared emission at 60 μm (contours). Part (d) shows an overlay of the infrared emission at 8.3 μm (grey-scale) and the radio continuum emission at 1420 MHz (contours). The image at 8.3 μm reveals an arc-shaped feature, 5 arcmin in width, which delineates the border of the H II region towards higher galactic longitudes and lower galactic latitudes, and coincides with a similar feature seen at 60 μm. No emission in the *MSX* band A is detected close to HD 24431. It is very likely that the image at 8.3 μm shows radiation from polycyclic aromatic hydrocarbons (PAHs), which can survive in the neutral gas around H II regions (Hollenbach & Tielens 1997) but not inside the ionized regions. Thus, this emission traces a photodissociated region (PDR) lying on the outskirts of LBN 148.11–0.45.

NVSS J035327+533601 also has a bright counterpart at 8.3 μm. No significant emission at 8.3 μm is detected in the rest of the area. We note that band E is free of emission in the whole area.

The *IRAS* (*HIRES*) image at 12 μm (not shown here) presents the same spatial distribution as the 8.3-μm image, as the filter responses of the A and 12-μm bands are similar (Egan & Price 1996). These bands are detecting dust with the same physical conditions.

Table 5 lists flux densities at 60 and 100 μm, dust temperatures, and dust masses associated with LBN 148.11–0.45 and SH 148.83–0.67. The parameter n is related to the dust absorption efficiency ($\kappa_\nu \propto \nu^n$). The dust temperature was estimated for n in the range 1 to 2. The infrared emission related to LBN 148.11–0.45 was split into three regions to obtain the physical parameters of the associated dust. The first region involves the infrared emission associated with the central part of the H II region (region a), the second one is the arc-shaped structure (region b), and the third one is the extended emission coincident with NVSS J035327+533601 (region c). Region (d) corresponds to the H II region as a whole. Uncertainties in listed dust masses originate in the adopted distance error and in different infrared background emissions. No significant difference in dust colour temperature is apparent among the various sections of LBN 148.11–0.45. Derived dust

Table 4. Physical parameters of H II regions.

SH 148.83–0.67	
Related star	HD 24431
Size (arcmin)	60 × 54
Adopted distance (kpc)	1.0 ± 0.2
Size (pc)	17.5 × 15.7
Radius (pc)	8.3
S_{1420} (Jy)	7.2 ± 0.2
S_{408} (Jy)	6 ± 0.3
S_{2700} (Jy)	3.7 ± 1.8
α	−0.20 ± 0.12
T_e (K)	8000 ± 2000
EM (pc cm^{-6})	520 ± 120
$f = 1$	
n_e (cm^{-3})	6 ± 1
M_i ($M_\odot$)	420 ± 170
$f = 0.1$–0.3	
n_e (cm^{-3})	15 ± 4
M_i ($M_\odot$)	180 ± 90
LBN 148.11–0.45	
Related stars	HD 24094, ALS 7793
Size (arcmin)	30 × 24
Adopted distance (kpc)	1.0 ± 0.2
Size (pc)	8.7 × 7.0
Radius (pc)	3.9
S_{1420} (Jy)	3.2 ± 0.1
S_{408} (Jy)	1.90 ± 0.07
S_{2700} (Jy)	2.3 ± 1
α	+0.13 ± 0.1
T_e (K)	10000
EM (pc cm^{-6})	1000 ± 160
$f = 1$	
n_e (cm^{-3})	12 ± 1
M_i ($M_\odot$)	70 ± 25

temperatures for SH 148.83–0.67 and LBN 148.11–0.45 are typical for H II regions.

4.3 The H I gas emission distribution

In order to find possible H I structures associated with the ionized regions, the H I data-cube was carefully examined within the velocity range from −165 to +45 km s^{-1} (all velocities in this paper are with respect to the local standard of rest).

The average H I spectrum corresponding to a region of 2 × 2 deg^2 in size centred at (l, b) = (148°29′, −0°19′) is displayed in Fig. 4 to facilitate visualization of the large-scale characteristics of the H I in the area. The H I profile shows the presence of significant emission covering the velocity range from −80 to +10 km s^{-1}. Three main H I components can be distinguished. According to circular galactic rotation models (Brand & Blitz 1993), components centred at +4, −32 and −56 km s^{-1} should be located at kinematical distances of $\lesssim$1, 4 ± 1 and 9 ± 2 kpc, respectively. These features are probably related to emission from the local and the Perseus spiral arms (Georgelin & Georgelin 1976).

The H I profile presents a minimum at ∼ −15 km s^{-1}. The circular galactic rotation model predicts a kinematical distance of ∼1.6 ± 0.8 kpc for gas at this velocity, compatible with distance estimates for HD 24431 (see Table 1). In order to look for cavities and holes that may be associated with HD 24431 and HD 24094 we have meticulously inspected the velocity interval [+6, −50] km s^{-1}.

Fig. 5 shows the H I emission within the velocity interval +1.6 to −31.6 km s^{-1} in steps of 3.3 km s^{-1}. Each image is the average of four consecutive H I maps. In order to facilitate the display of the images, a constant background, equal to the mean value of each image within a box of 2 × 2 deg^2 in size centred at (l, b) = (148°29′, −0°19′) was subtracted from every map. The H I gas distribution is complex, and, as a consequence, the identification of the neutral gas associated with the ionized regions is hard to establish. We will discuss each case separately, along with the case of an H I shell centred at (l, b) = (149°0′, −1°30′).

4.3.1 H I gas related to LBN 148.11–0.45

An inspection of Fig. 5 shows that H I gas related to LBN 148.11–0.45 is detected within the velocity range from +1.6 to −15.1 km s^{-1}. At +1.6 km s^{-1}, a region of enhanced H I emission is seen partially coincident with the H II region. This feature consists of a faint elongated H I cloud centred at (l, b) = (148°10′, −0°15′) that extends for 30 arcmin at a position angle of ∼45°. Within the velocity interval from −1.6 to −5.2 km s^{-1}, H I gas is clearly seen surrounding the H II region near (l, b) ≈ (148°15′, −0°15′). In the velocity range from −5.2 to −11.8 km s^{-1}, a patchy envelope encircles the H II region almost completely. At ∼ −8.5 km s^{-1}, the brightest section of the H I structure surrounds the H II region towards $b \sim -0°40'$. The envelope is hardly identifiable at $v \lesssim -15.0$ km s^{-1}. At $v \approx -22.0$ km s^{-1}, HD 24094 and ALS 7793 are seen projected onto a bright H I filament that runs along a position angle of ∼30°across the area.

Fig. 6 shows the H I emission in the velocity range from −1.5 to −11.4 km s^{-1} (part a), and an overlay of the 1420-MHz continuum emission and the H I image (part b). H I gas most probably related to LBN 148.11–0.45 is clearly seen in (a), where the H I envelope is identified. We believe that the H I gas that encompasses LBN 148.11–0.45 represents an atomic gas shell associated with the ionized region. H I gas projected onto the central part of the H II region, which is detected within the velocity interval +1.5 to −5.2 km s^{-1}, may represent part of the receding cap of the envelope.

4.3.2 H I gas related to SH 148.83–0.67 and SH 149.25–0.0

The identification of neutral atomic gas related to these features is particularly difficult.

Fig. 5 shows a low-emission region surrounded by an almost complete shell centred at (l, b) = (148°50′, −0°35′), which can be identified in the velocity range from −22.0 to −32.0 km s^{-1}.

Fig. 7 shows the H I emission averaged in the velocity range from −25.0 to −28.0 km s^{-1}, where this feature is better defined. The cavity and the outer shell, 1.8 × 1.3 deg^2 in size, are shown in Fig. 7(a). The borders of the cavity are defined by the contour line corresponding to 70 K at $b \leqslant -0°30'$ and by the contour line corresponding to 60 K at $b \geqslant -0°30'$. Fig. 7(b), which displays a superposition of the H I and optical images, shows that the optical arc-like feature at (l, b) = (148°45′, −0°50′) appears projected onto the cavity. The faint optical emission at (l, b) = (149°, −0°20′) is seen within the cavity. The comparison between the H I and optical emission suggests that this H I shell is related to SH 148.83–0.67.

A bright H I filament running along the complete interval of galactic longitudes at a position angle of 30° can be easily distinguished at ∼ −22.0 km s^{-1} (Fig. 5), with HD 24431 projected onto the H I

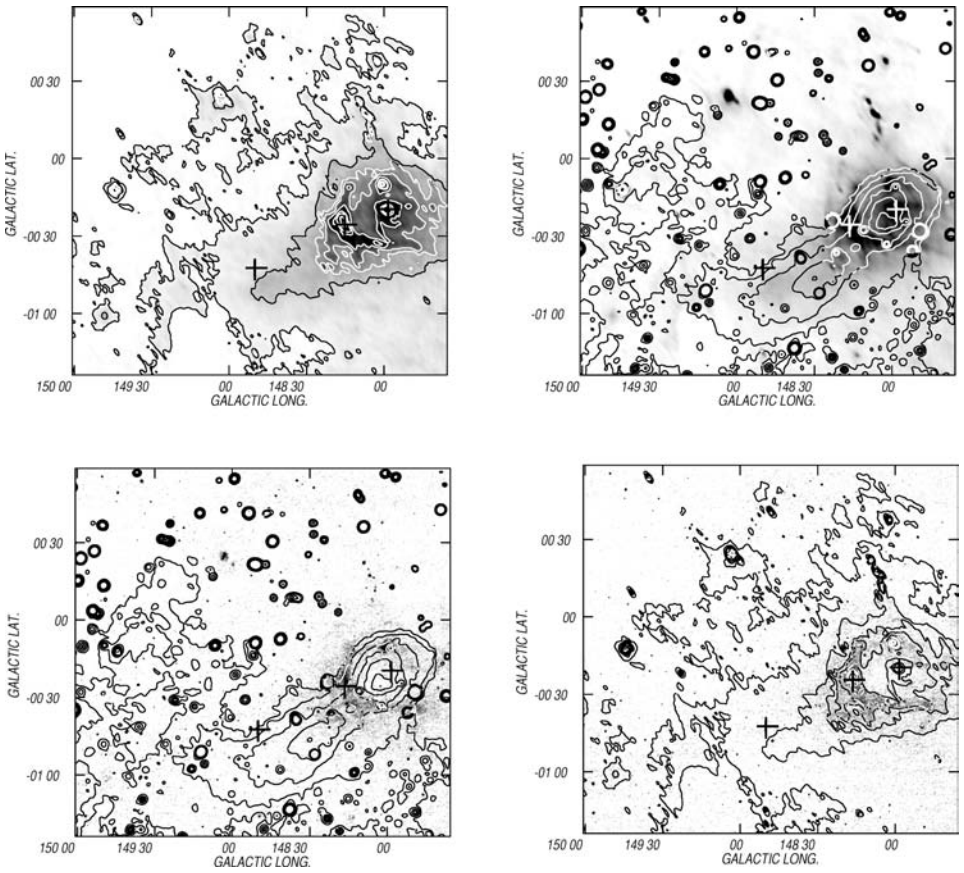

Figure 3. (a) Image at 60 μm in grey-scale and contour lines. Contour lines are 10, 15, 20, 25, 35, 50, 60, 100, and 140 MJy ster^{-1}. Grey-Scale is from 9.00 to 40.00 MJy ster^{-1}. (b) Overlay of the 60-μm image (grey-scale) and 1420-MHz emission (contours). Contour levels are from 5.2 to 6.1 K in steps of 0.1 K. (c) 1420-MHz emission (contours) superimposed on the 8.3-μm image (grey-scale). Grey-scale corresponds to 600×10^{-9} to 1400×10^{-9} W m^{-2} ster^{-1}. (d) Overlay of the 8.3-μm image (grey-scale) and 60-μm emission (contours). The crosses mark the positions of HD 24431, ALS 7793, and HD 24094.

Table 5. Parameters of the interstellar dust associated with LBN 148.11–0.45 and SH 148.83–0.67.

H II region	$S_{60\,\mu m}$ (Jy)	$S_{100\,\mu m}$ (Jy)	T_d (K) ($n = 1.0$–2.0)	$M_d(M_\odot)$ $n = 1.0$	$n = 2.0$
LBN 148.11–0.45 (a)	680	1410	32 ± 3	0.2 ± 0.1	0.8 ± 0.3
LBN 148.11–0.45 (b)	910	2470	29 ± 3	0.6 ± 0.3	2.0 ± 0.9
LBN 148.11–0.45 (c)	260	740	29 ± 3	0.2 ± 0.1	0.6 ± 0.3
LBN 148.11–0.45 (d)	2900 ± 100	8100 ± 300	29 ± 3	0.4 ± 0.2	1.5 ± 0.6
SH 148.83–0.67	620 ± 180	1750 ± 450	29 ± 3	2.0 ± 0.8	7.0 ± 3.0

filament. Thin H I areas surround the bright knots seen in the optical image near $(l, b) = (148°40', -0°45')$, suggesting that the H I gas at this velocity interacts with the nebula.

For a systemic velocity of ~ -27 km s^{-1}, the circular galactic rotation model (see Fig. 4) predicts a kinematical distance of $\sim 3.3 \pm 0.8$ kpc, assuming a velocity dispersion of 6 km s^{-1}. The derived distance is larger than spectrophotometric distance estimates for HD 24431 (see Table 1). Based on the spectrophotometric distance to this star, we adopt $d = 1.0 \pm 0.2$ kpc as the distance to SH 148.83–0.67 and the surrounding H I shell.

The other H I structure in the area is centred at $(l, b) = (149°15', +0°25')$ at $v = -15.1$ km s^{-1}, and is $\sim$60 arcmin in diameter. The structure can be followed within a velocity range from -12.0 to -18.4 km s^{-1}. At ~ -15 km s^{-1}, this feature presents its largest angular size, and its borders are better defined than at other velocities (Fig. 8a). For gas at this velocity, the analytical fit given by Brand & Blitz (1993) predicts a kinematical distance of $d = 1.8 \pm 0.8$ kpc. The comparison with the radio continuum emission at 1420 MHz reveals that the weak radio emission at $(l, b) = (149°15', + 0°20')$, related to SH 149.25–0.00, is seen projected onto the innermost part of the cavity, suggesting that the H I structure is linked to it.

4.3.3 An H I shell centred at (l, b) = (149°0′, −1°30′)

The analysis of the H I emission allows identification of an H I structure within the velocity range -5.2 to -15.1 km s^{-1}, centred at $(l, b) = (149°0', -1°30')$, with a systemic velocity of ~ -12 km s^{-1}. The open cluster NGC 1444, at a distance of 1.2 kpc (see Section 1), is placed near the border of the H I hole. The kinematical distance of

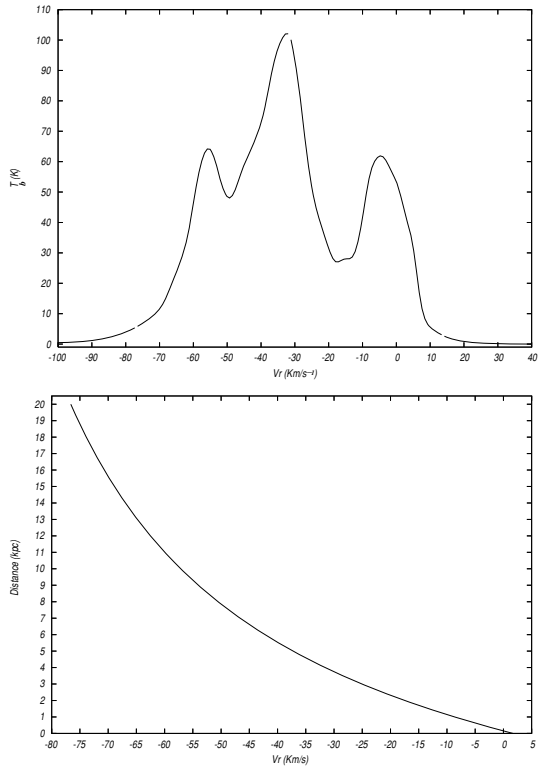

Figure 4. (a) Average H I profile within a region of $2 \times 2\,\mathrm{deg}^2$ in size, centred at $(l, b) = (148^\circ29', -0^\circ19')$. (b) Kinematical distance versus radial velocity plot derived from the analytical fit to the rotation curve by Brand & Blitz (1993).

the shell is compatible with the optical distance to the cluster. The structure is $\sim 2.2 \times 1.5\,\mathrm{deg}^2$ in size and is shown in Fig. 8(b).

4.3.4 Physical parameters of the H I structures

Table 6 lists the main data of the neutral atomic structures identified in the region: the (l, b) centroid of the H I shells, the velocity interval spanned by the structures, the systemic and expansion velocities, and the kinematical and adopted distances. The expansion velocity was estimated from the velocity range spanned by the H I feature as $(v_2 - v_1)/2 + 1.0$. The size of the H I structures was derived from the position of the maxima in the shells. The radius, R_s, is defined as half the geometric mean of the axes of the H I structure. The neutral atomic mass corresponds to the mass excess in the shell. It was obtained within a circle of radius R_e, assuming that the gas is optically thin, and includes a He abundance of 10 per cent. The neutral atomic mass associated with the H I shell probably linked to SH 149.25–0.00 is difficult to establish.

4.4 The molecular gas emission distribution

The analysis of the ^{12}CO emission distribution in the region shows the presence of molecular gas associated with LBN 148.11–0.45 within the velocity range from -0.65 to -11.1 km s^{-1}. Fig. 9(a) shows an overlay of the ^{12}CO emission distribution within the velocity range $[-3.2, -4.5]$ km s^{-1} (contours) and the infrared emission at 60 μm (grey-scale). The molecular cloud at $l = (148^\circ25')$ delineates strikingly well the border of the PDR detected at 8.3 μm. Note that this CO cloud encompasses the brightest H I emission arc detected at $v = -1.6$ km s^{-1} (Fig. 5), suggesting that the thin H I filament could originate in the photodissociation of the molecular gas.

CO emission seen towards the central part of the H II region LBN 148.11–0.45 probably originates from behind the ionized region.

Fig. 9(b) shows the ^{12}CO emission distribution in the velocity range $[-0.65, -11]$ km s^{-1} superimposed onto the VTSS image. The ^{12}CO gas emission at $(l, b) = (148^\circ25', -0^\circ40')$ coincides with the faint optical emission region that separates the optically bright regions SH 148.83–0.67 and LBN 148.11–0.45. The slight distortion in the molecular clump at $(l, b) = (148^\circ25', -0^\circ40')$ following the border of SH 148.83–0.67, and the morphological correlation among the optical, radio continuum, and ^{12}CO emissions indicate that the molecular gas is interacting with the ionized material.

The bottom panels of Fig. 9 show the ^{12}CO emission within the velocity interval -3.1 to -17.1 km s^{-1} and a superposition of the CO and H I gas distributions in the region of the H I shell centred at $(l, b) = (149^\circ0', -1^\circ30')$. The morphological correspondence between the H I and CO emissions reveals that this H I shell has a clear molecular counterpart.

The open cluster NGC 1444, marked in Fig. 9 by a circle, is seen projected close to the border of the CO and H I emission rings.

Towards the region under study, identification of molecular structures related to the ionized regions is easier than recognition of the associated H I structures, as expected given confusion effects in the line of sight.

Table 6 summarizes the physical parameters of the molecular clouds associated with the ionized and neutral regions. The H_2 column density (N_{H_2}) was derived from the ^{12}CO data, taking into account the empirical relation between the integrated emission $W_{CO}(= \int T\,dv)$ and N_{H_2}. We adopted $N_{H_2} = (1.9 \pm 0.3) \times W_{CO} \times 10^{20}$ cm^{-2} (K km s^{-1})$^{-1}$, obtained from γ-ray studies of molecular clouds in the Cepheus Flare (Digel et al. 1996; Grenier & Lebrun 1990). To derive the molecular mass associated with LBN 148.11–0.45, we took into account the region enclosed by the contour level of 1.5 K centred at $(l, b) = (148^\circ10', -0^\circ20')$. For the case of the molecular mass associated with the H I shell centred at $(l, b) = (149^\circ0', -1^\circ30')$, we considered the region enclosed by the dash–dot line (Fig. 9). Errors in the derived molecular masses arise from uncertainties in distance and in N_{H_2}.

The ambient density was derived by distributing the ionized, neutral atomic and molecular masses over a sphere of radius R_e. For the case of LBN 148.11–0.45, $R_e = 31$ arcmin ($\equiv$9 pc), which corresponds to the region showing CO emission.

The comparison between the low neutral atomic mass related to LBN 148.11–0.45 and the associated molecular mass suggests that the H I mass originated in the photodissociation of the molecular gas. This region is clearly evolving in a highly dense ambient medium.

5 THE ORIGIN OF THE STRUCTURES

5.1 SH 148.83–0.67

We can estimate the number of UV photons N_{Ly-c} (s^{-1}) necessary to ionize the gas in the H II region from the radio continuum results, and we compare our estimate with the UV photon flux emitted by the exciting star, N_*, as derived from stellar atmosphere models. From the expression for Stromgren's sphere (see Spitzer 1978), and adopting a radius of 8.3 pc for the H II region SH 148.83–0.67 and the electron density listed in Table 4 corresponding to $f = 1$, we derived $\log N_{Ly-c} = 47.9$.

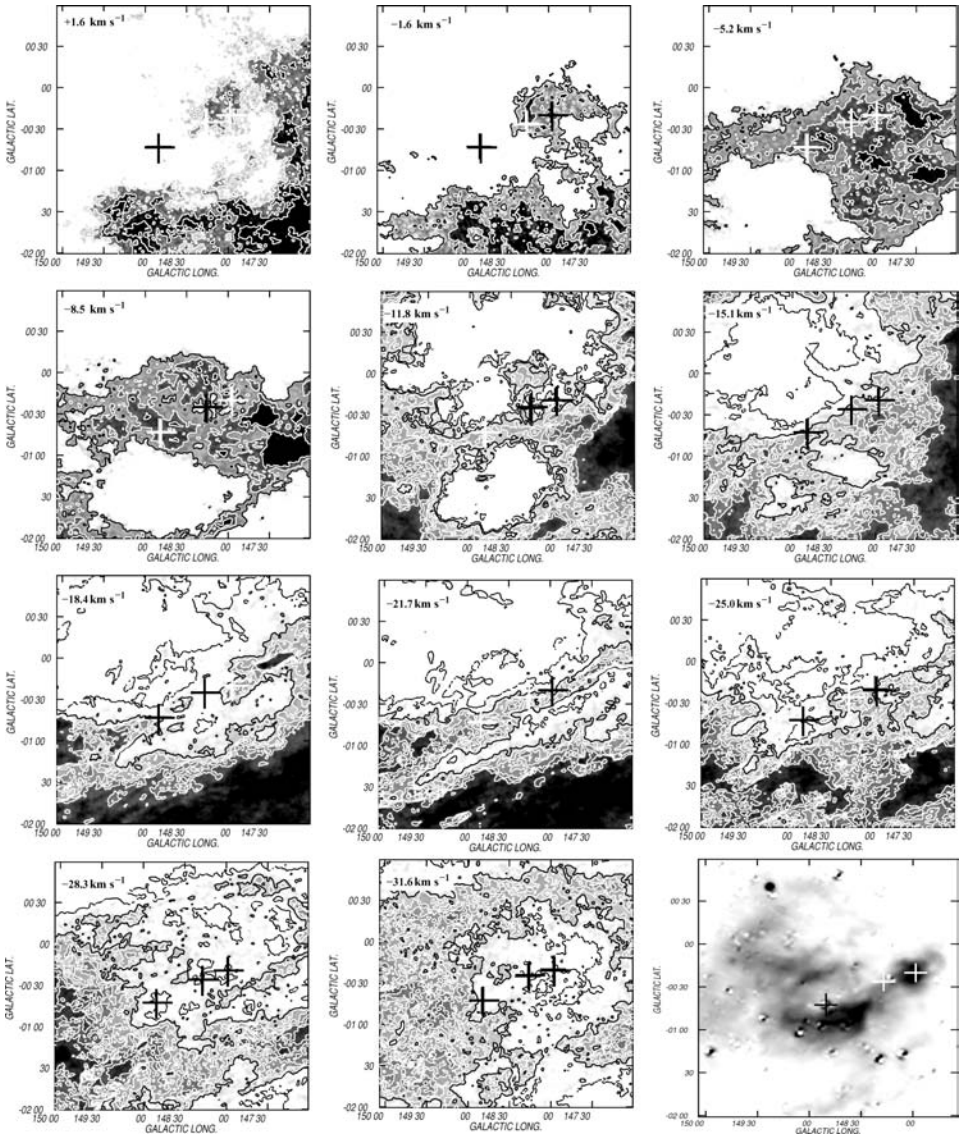

Figure 5. H I emission distribution in the velocity range from +1.6 to −31.6 km s^{-1}. The crosses mark the positions of HD 24431, ALS 7793, and HD 24094. The central velocity of each map is indicated in its upper left corner. Contour levels for maps within the velocity interval [+1.6, −11.8] km s^{-1} are from 4 to 16 K in steps of 4 K. Contour levels for maps within the velocity interval [−15.1, −31.6] km s^{-1} are from −8 to 16 K in steps of 4 K. The grey-scale for maps having velocities of +1.6 km s^{-1} and −1.6 km s^{-1} is from 0 K to 10 K. The grey-scale for the rest of the maps is from −10 K to 30 K. The optical image of Sh2-205 is shown in the bottom right corner. Darker regions mean brighter areas.

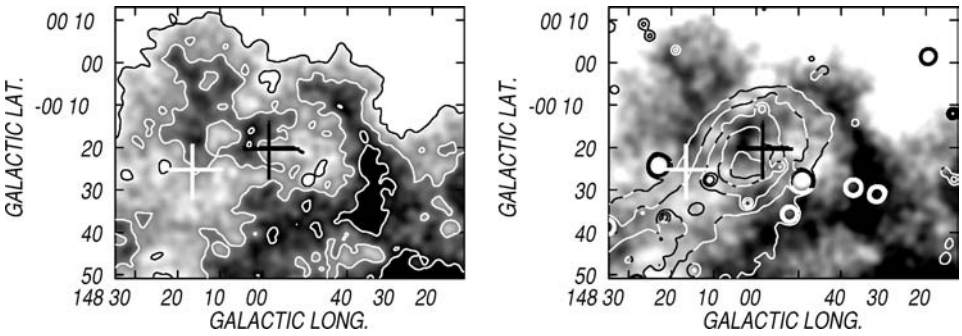

Figure 6. (a) H I emission distribution towards LBN 148.11–0.45 within the velocity range −1.5 to −11.4 km s^{-1}. The crosses indicate the positions of ALS 7793 and HD 24094. The grey-scale is from 60 to 70 K. Contour levels are from 60 to 75 in steps of 5 K. (b) Overlay of the H I emission shown in the left panel (grey-scale) and the radio continuum image at 1420 MHz (contour lines). Contour levels are from 5.3 to 6.1 K in steps of 0.2 K. Darker regions mean brighter areas.

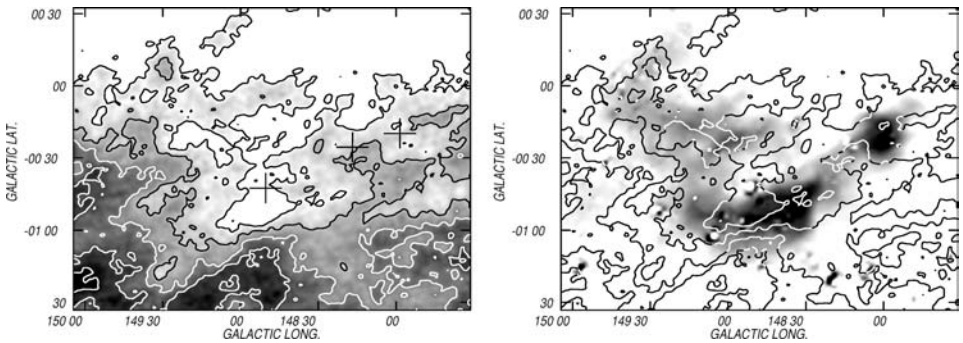

Figure 7. (a) H I emission distribution for the structure probably related to SH 148.83–0.67 within the velocity range −25.0 to −28.0 km s^{-1}. The grey-scale is from 60 to 100 K. The contour levels are 60 to 100 K in steps of 10 K. The crosses indicate the positions of HD 24431, ALS 773, and HD 24094. (b) Overlay of the H I emission distribution (contour lines) and the VTSS image (grey-scale). Darker regions mean brighter areas.

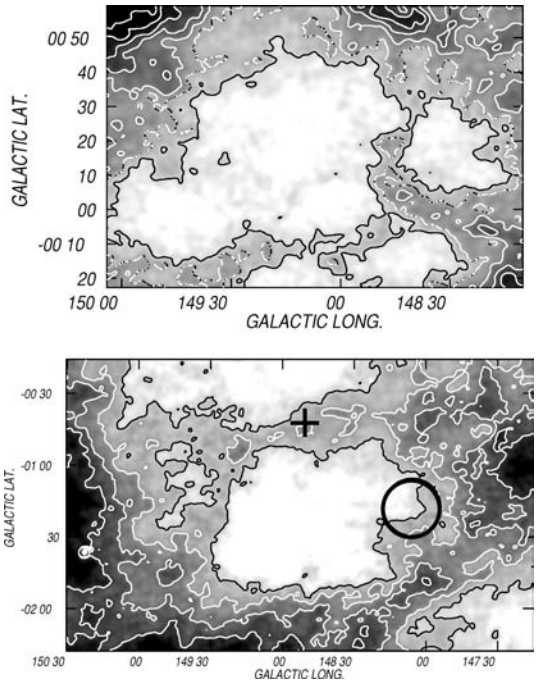

Figure 8. (a) H I emission distribution for the neutral atomic gas structure probably related to SH 149.25–0.0 within the velocity range −13.4 to −16.7 km s^{-1}. The grey-scale is 15 to 45 K. The contour levels are 10, and from 20 to 50 K in steps of 5 K. (b) H I emission distribution within the velocity interval from −3.1 to −17.1 km s^{-1} showing the H I structure at (l, b) = (149°0′, −1°30′). The contour levels are from 50 to 65 K in steps of 5 K. The positions of HD 24431 and NGC 1444 are indicated by a cross and a circle, respectively. Darker regions mean brighter areas.

Following Smith, Norris & Crowther (2002) and Martins, Schaerer & Hillier (2005), the number of Lyman continuum photons emitted by an O9 III star is in the range logN_* = 47.9–48.4, indicating that HD 24431 can maintain SH 148.83–0.67 ionized if a small amount of interstellar dust is related to the structure (Inoue 2001). Indeed, the lack of infrared emission related to this H II region suggests that little interstellar dust is present (see also Table 5).

To investigate whether the ring-like structure originated in the action of the stellar winds of HD 24431 on the surrounding gas, we will estimate the energy conversion efficiency, ϵ, defined as the ratio between the kinetic energy E_k in the shell and the mechanical energy supplied by the stellar wind E_w.

To evaluate the kinetic energy in the expanding shell, $E_k = 0.5MV^2_{exp}$, we consider that the ionized, H I, and molecular gas expand at V_{exp}. The kinetic energy is found to be $E_k = 2.3 \times 10^{47}$ erg.

A rough estimate of the stellar wind energy of HD 24431 can be obtained by adopting a mass-loss rate of $\dot{M} = 1 \times 10^{-7}$ M$_\odot$ yr^{-1} (Chlebowski & Garmany 1991) and a terminal velocity of V_w = 2000 km s^{-1} (Prinja et al. 1990). We assume that this wind blew during the dynamical age of the bubble, $t_d = 0.55\,R_s/V_{exp}$ (McCray 1983). For the values listed in Table 6, $t = 1.1 \times 10^6$ yr. The lifetime in the main sequence can be considered as an upper limit to this time. From Schaller et al. (1992), $t = 4.0 \times 10^6$ yr. For t = (1.1–4.0) × 10^6 yr, we estimate $E_w = 0.5\,\dot{M}\,V_w^2\,t$ = (5–16) × 10^{48} erg.

The parameter ϵ = 0.015–0.05, similar to values derived for other interstellar bubbles (Cappa, Niemela & McClure-Griffiths 2003), indicating that SH 148.83–0.67 probably originated in the stellar winds of the O9 III star.

5.2 LBN 148.11–0.45

Adopting the radius and electron density derived for this region from Table 4, we estimate that the UV photon flux necessary to ionize the gas is $log\ N_{Ly\text{-}c} = 47.7$. Clearly, this UV photon flux is higher than that provided by HD 24094 (B8V) and ALS 7793 (BIV). To look for additional sources of ionizing photons associated with the H II region, we investigated the presence of main-sequence O-type stars, which may contribute to the ionization of the H II region, using the 2MASS data base. We identified the main-sequence candidates based on the position of the sources in the colour–magnitude (CMD) and the colour–colour (CCD) diagrams according to the q parameter. Following Hanson, Howarth & Conti (1997), the parameter q is defined as

$$q = (J - H) - 1.83(H - Ks). \quad (1)$$

Main-sequence stars have q-values in the range −0.15 to 0.10. Using this selection criterion, we found 28 candidates to be main-sequence stars in the region of LBN 148.11–0.45. Fig. 10 shows the spatial distribution of these sources superimposed onto the image at 8.3 μm, and the CMD. Most of the sources have *Ks* magnitudes greater than 10 mag, suggesting that they are foreground late-type stars (later than B1 V). HD 24094, indicated in Fig. 10 as a filled circle, has values ($H - Ks$, Ks) = (0.023,7.35), corresponding to an O-type star (O8.5 or O9) with A_v = 10 mag, which is different from the B-type star determination by Duerbeck (1997). Were HD 24094 an O8.5 V–O9 V star, it would supply a UV photon flux $N_* = 1 \times 10^{48}$ s^{-1}

Table 6. Parameters of H I and ^{12}CO structures.

Related ionized regions	LBN 148.11–0.45	SH 148.83–0.67	–	Sh 149.25–0.0
Neutral H I shells				
(l, b) centroid	$147°55', -0°20'$	$148°50', -0°35'$	$149°0', -1°30'$	$149°15', +0°25'$
Velocity interval v1,v2 (km s^{-1})	+1.6, −18.0	−22, −32	−5, −15	−20, −12
Systemic velocity (km s^{-1})	-9 ± 1	-27 ± 1	-12 ± 1	-15 ± 1
V_{exp} (km s^{-1})	11	7	7	6
Kinematical distance d (kpc)	1.3	3.3	1.5	1.8
Adopted distance (kpc)	1.0 ± 0.2	1 ± 0.2	1.0 ± 0.2	1.0 ± 0.2
Size of the H I structure ($r_1 \times r_2$) (arcmin)	51×49	105×80	129×90	60×60
Size of the H I structure ($r_1 \times r_2$) (pc)	15×14	31×23	38×26	17×17
Radius R_s (pc)	7.2	13.4	15.7	8.5
R_e (arcmin)	25	27	56	–
Neutral atomic mass ($M_\odot$)	65 ± 25	300 ± 120	1600 ± 640	–
Molecular gas				
Velocity interval v1,v2 (km s^{-1})	−0.65, −11.1	–	−0.65, −11.1	–
W_{CO} (K km s^{-1})	41	–	9	–
Mean H_2 column density (10^{21} mol$_{H_2}$ cm^{-2}	8 ± 0.8	–	2 ± 0.2	–
Mass ($10^4 \times M_\odot$)	6.0 ± 3.0	–	2.6 ± 1.3	–
Ambient density (cm^{-3})	∼800	∼2	∼70	

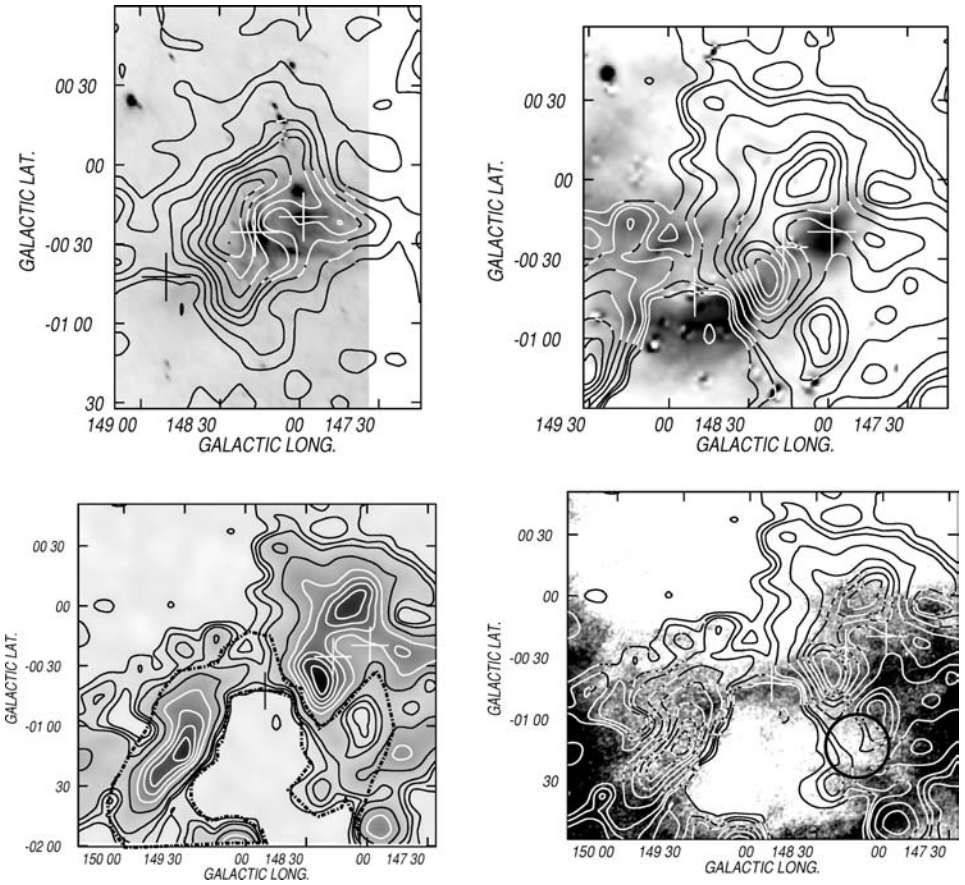

Figure 9. ^{12}CO emission distribution. (a) Overlay of the integrated ^{12}CO emission in the velocity range from −3.2 to −4.5 km s^{-1} (contour lines) and the 60-μm image (grey-scale). Contours levels are 0.15 ($\equiv 3\sigma$), 0.5, 1, 1.5 K, from 2 to 6 K in steps of 1 K, and from 6 to 16 K in steps of 2 K. (b) ^{12}CO emission integrated in the velocity interval [−0.65, −11.1] km s^{-1} superimposed onto the VTSS Hα image (grey-scale). (c) ^{12}CO emission emission integrated in the velocity interval [−0.65, −11.1] km s^{-1}. The molecular mass was derived within the area marked by the dash–dot line. (d) Overlay of the ^{12}CO emission and the H I emission distributions within the velocity range from −3.1 to −17.1 km s^{-1} (grey-scale). The contour levels indicated in the lower panels are the same as those displayed in (b). The positions of HD 24431, ALS 7793, and HD 24094 are indicated by crosses.

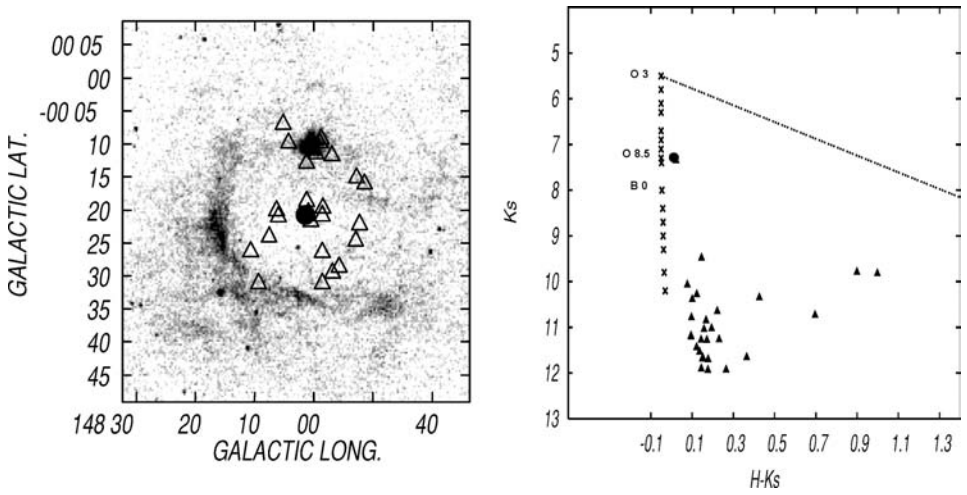

Figure 10. (a) Spatial distribution of the main-sequence star candidates from the 2MASS PSC (triangles) superimposed onto the image at 8.3 μm of LBN 148.11–0.45. (b) Near-infrared colour–magnitude diagram of the main-sequence star candidates shown in (a). The sources are represented by triangles. The position of the main sequence is shown by crosses. We have adopted a distance of 1.0 kpc. The dashed line represents the reddening curve for an O3 star. The filled circle indicates the position of HD 24094 in both panels.

(Martins et al. 2005), enough to explain the ionization of the H II region. Spectroscopic data are needed to confirm this point.

Note that a number of B-type star candidates are projected onto NVSS J035327+533601.

We can roughly estimate the age of the H II region LBN 148.11–0.45 from the expression (12-20) in Spitzer (1978), which considers the expansion of an H II region with time. The radius of the H II region at the beginning of the expansion phase, $R_{\rm i}$, can be derived from the expression for Strongrem's sphere, adopting an electron density equal to the ambient density (see Table 6) and log $N_{{\rm Ly}-c} = 47.7$. For $R_{\rm i} = 0.35$ pc and adopting the present radius of $R_{\rm i} = 7.2$ pc, the age of the H II region is 4×10^6 yr.

5.3 Shell centred at $(l, b) = (149^\circ 0', -1^\circ 30')$

The question that arises is whether this neutral gas structure is physically related to NGC 1444. The estimated age of this cluster is in the range (25–41) $\times 10^6$ yr (Lynga 1983, 1987). The spectral type of its earliest star is B2 (Lynga 1983), and four blue stragglers were found to be related to it (Ahumada & Lapasset 1995). Leisawitz (1990) carried out a molecular survey around open clusters and found molecular clouds within the velocity range [−0.4, −26] km s^{-1} that were probably associated with NGC 1444. Clouds labelled by Leisawitz (1990) as I and E centred at $(l, b) = (149^\circ 12', -0^\circ 24')$ and $(l, b) = (149^\circ 36', -1^\circ 6')$ with mean radial velocities of −4.5 and −8.1 km s^{-1}, respectively, coincide in position and velocity with the CO ring shown in Fig. 9. No other OB stars projected onto the cavity were found in the literature. The origin of this shell is still an open question.

6 SUMMARY

We have examined the ISM surrounding Sh2-205. We based our study on radio continuum data at 408 and 1420 MHz, 21-cm H I line emission data from the Canadian Galactic Plane Survey, ^{12}CO data from the survey by Dame et al. (2001), and *IRAS* (*HIRES*) and *MSX* data.

The main findings can be summarized as follows.

(1) Sh2-205 can be separated into three independent structures, termed SH 149.25–0.00, SH 148.83–0.67, and LBN 148.11–0.45. To obtain the physical properties of these optical nebulae we adopted a distance of 1.0±0.2 kpc.

(2) We conclude that SH 148.83–0.67 is an interstellar bubble powered by the energetic winds of HD 24431. Low infrared emission is detected in this region. The H I shell related to SH 148.83–0.67 is identified in the velocity range from −22 to −32 km s^{-1}. It is 31 × 23 pc^2 in size and expands at 6 km s^{-1}. The electron density and the associated ionized mass are 15 ± 4 cm^{-3} and 180 ± 90 M$_\odot$, respectively, adopting a filling factor $f = 1$. The associated neutral atomic mass is 65 M$_\odot$.

(3) LBN 148.11–0.45 is a classical H II region. The optical, mid- and far-infrared emissions reveal that dust and gas are well mixed in this region. The dust temperature is ∼29 K, typical of H II regions. Molecular gas within the velocity range [−0.65, −11.1] km s^{-1} is found to be associated with the H II region. We estimated a molecular mass of 60×10^3 M$_\odot$. The distribution of the emission in the *MSX* band A encircles the H II region and correlates with the molecular emission, indicating the presence of a PDR. Neutral atomic gas in the velocity range [+1.6, −18.0] km s^{-1} is related to LBN 148.11–0.45. H I gas with velocities in the range from +1.6 to −5.2 km s^{-1} is seen projected onto the central part of the H II region, which may represent part of the receding cap of the envelope. The H I structure is 15 × 14 pc^2 in size and expands at about 9 km s^{-1}. The associated neutral atomic mass is 300 M$_\odot$. The electron density and ionized mass are 12 ± 1 cm^{-3} and 70 ± 25 M$_\odot$, respectively. The H II region is evolving in a dense ISM. We estimate that the H II region has been expanding for 4×10^6 yr.

The ionizing source of LBN 148.11–0.45 remains uncertain. The earliest spectral-type stars seen in projection onto this region are ALS 7793 (B1 V) and HD 24094. Duerbeck (1997) determined a B8 V spectral type for HD 24094. However, results from the 2MASS point-source catalogue showing main-sequence stars in the area of the nebula suggest that HD 24094 is an O8.5–O9 star. A star with this spectral type would provide the necessary UV photon flux to

keep the H II region ionized. High-quality spectroscopic data are needed to elucidate this point.

(4) An H I structure within the velocity range −5.2 to −15.1 km s^{-1} was identified centred at (l, b) = (149°0′, −1°30′). This shell correlates morphologically with molecular gas emission detected in the velocity range from −0.65 to −11.1 km s^{-1}. The neutral and molecular masses are 1600 $M_\odot$ and 20 × 10^3 $M_\odot$, respectively. Possible progenitors of this structure are the stellar members of NGC 1444.

(5) An H I shell was also found to be possibly associated with SH 149.25–0.00. The neutral atomic structure is expanding at 6 km s^{-1} and is about 17 pc in diameter. The radio continuum emission is too faint to allow us to determine the physical properties of this nebula. No early-type stars that could have been responsible for the ionization and expansion of SH 149.25–0.00 were found in the literature.

(6) A relatively large number of main-sequence candidates were found in the region of LBN 148.11–0.45 from the 2MASS point-source catalogue. Particularly interesting are the main-sequence candidates projected onto NVSS J035327+533601 at (l, b) = (148°0′, −0°10′).

Finally, the presence of a photodissociation region at the interface between the molecular material and the ionized gas in LBN 148.11–0.45, strikingly bordering the ionized region, is suggestive of the existence of regions of active stellar formation. This suggestion is reinforced by the high-density medium in the area where the H II region is evolving.

The observed scenario favours the conditions for the collect and collapse process (Elmegreen & Lada 1977), as was found by Deharveng et al. (2003) for Sh2-104. In a forthcoming paper, we will analyse the stellar formation activity in the area.

ACKNOWLEDGMENTS

We thank Dr T. Dame for making his CO data available to us. We are grateful to the anonymous referee for his helpful suggestions. This project was partially financed by the Consejo Nacional de Investigaciones Científicas y Técnicas (CONICET) of Argentina under project PIP 5886/05, Agencia PICT 14018, and by UNLP under project 11/G072. The Digitized Sky Survey (DSS) was produced at the Space Telescope Science Institute under US Government grant NAGW-2166.

REFERENCES

Ahumada J., Lapasset E., 1995, A&AS, 109, 375
Blitz L., Fich M., Stark A. A., 1982, ApJS, 49, 183
Brand J., Blitz L., 1993, A&A, 275, 67
Cappa C., Niemela V. S., McClure-Griffiths N. M., 2003, in Arthur S. J., Henney W. J., eds, Rev. Mex. Astron. Astrofis. Ser. Conf. Vol. 15, Winds, Bubbles, and Explosions. UNAM, Mexico, p. 47
Chlebowski T., Garmany C. D., 1991, ApJ, 368, 241
Condon J. J., Cotton W. D., Greisen E. W., Yin Q. F., Perley R. A., Taylor G. B., Broderick J. J., 1998, AJ, 115, 1693
Cruz-González C., Recillas-Cruz E., Costero R., Peimbert M., Torres-Peimbert S., 1974, Rev. Mex. Astron. Astrofis., 1, 211
Dame T. M., Hartmann D., Thaddeus P., 2001, ApJ, 547, 792
Deharveng L., Zavagno A., Caplan J., Lefloch B., Salas L., Porras A., Cruz-González I., 2003, A&A, 408, L25-28
del Rio G., Huestamendia G., 1988, A&AS, 73, 425
Digel S. W., Lyder D. A., Philbrick A. J., Puche D., Thaddeus P., 1996, ApJ, 458, 561
Duerbeck H. W., 1997, Inf. Bull. Var. Stars, 4513, 1
Durgapal A. K., Pandey A. K., Mohan V., 1997, Bull. Astron. Soc. India, 25, 489
Egan M. P., Price S. D., 1996, AJ, 112, 2862
Elmegreen B. G., Lada C. J., 1977, ApJ, 214, 725
Fabricius C., Hog E., Makarov V. V., Mason B. D., Wycoff G. L., Urban S. E., 2002, A&A, 384, 180
Felli M., Churchwell E., 1972, A&AS, 5, 369
Fich M., Dahl G. P., Treffers R. R., 1990, AJ, 99, 622
Fürst E., Reich W., Reich P., Reif K., 1990, A&AS, 85, 691
Garmany C. D., Conti P. S., Chiosi C., 1982, ApJ, 263, 777
Georgelin Y. M., Georgelin Y. P., 1976, A&A, 49, 57
Gies D. R., 1987, ApJS, 64, 545
Goss W. M., Lozinskaya T., 1995, ApJ, 439, 637
Gregory P. C., Condon J. J., 1991, ApJS, 75, 1011
Grenier I. A., Lebrun F., 1990, ApJ, 360, 129
Hales S. E. G., Baldwin J. E., Warner P. J., 1988, MNRAS, 234, 919
Hanson M. M., Howarth I. D., Conti P. S., 1997, ApJ, 489, 698
Hiltner W. A., Johnson H. L., 1956, ApJ, 124, 367
Hollenbach D. J., Tielens A. G. G. M., 1997, ARA&A, 35, 179
Humphreys R. M., 1978, ApJS, 38, 309
Inoue A. K., 2001, AJ, 122, 1788
Lamers H. J. G. L. M., Leitherer C., 1993, ApJ, 412, 771
Lamers H. J. G. L. M., Cassinelli J. P., 1999, J. British Astron. Association, 109, 347
Leisawitz D., 1990, ApJ, 359, 319
Lindoff U., 1968, Arkiv för Astronomii, 5, 1
Lyder D. A., 2001, AJ, 122, 263
Lynds B. T., 1965, ApJS, 12, 163
Lynga G., 1983, Catalogue of Open Cluster Data, 3rd edn. Available through NSSDC, Greenbelt, MD
Lynga G., 1987, Catalogue of Open Cluster Data, 5th edn. Available through NSSDC, Greenbelt, MD
Martins F., Schaerer D., Hillier D. J., 2005, A&A, 436, 1049
McCray R., 1983, in Proc. Int. Astron. Un. Vol. 6 (A84-28901 12-90) Highlights of Astronomy. Reidel, Dordrecht, p. 565
Mezger P. D., Henderson A. P., 1967, ApJ, 147, 471
Moffat A., Puls J., 2003, in van der Hucht K., Herrero A., Esteban C., eds, Proc. IAU Symp. 212, A Massive Star Odyssey: From Main Sequence to Supernova. Astron. Soc. Pac., San Francisco, p. 773
Newberg H. J., Richards G. T., Richmond M., Fan X., 1999, ApJS, 123, 377
Osterbrock D. E., 1989, Astrophysics of Gaseous Nebulae and Active Galactic Nuclei. University Science Books, Mill Valley, CA
Prinja R. K., Barlow M. J., Howarth I. D., 1990, ApJ, 361, 607
Schaller G., Schaerer D., Meynet G., Maeder A., 1992, A&AS, 96, 269
Sharpless S., 1959, ApJS, 4, 257
Smith L. J., Norris R. P. F., Crowther P. A., 2002, MNRAS, 337, 1309
Spitzer L., 1978, Physical Processes in the Interstellar Medium. Wiley-Interscience, New York, NY
Taylor J. H., Manchester R. N., Lyne A. G., 1993, ApJS, 88, 529
Taylor A. R. et al., 2003, AJ, 125, 3145
Walborn N. R., 1973, AJ, 78, 1067
Weaver R., McCray R., Castor J., Shapiro P., Moore R., 1977, ApJ, 218, 377
Zdanavičius J., Černis K., Zdanavičius K., Straižys V., 2001, Baltic Astron., 10, 349

This paper has been typeset from a TEX/LATEX file prepared by the author.